Deep Resources Engineering 3 (2026) 100227

Contents lists available at ScienceDirect

Deep Resources Engineering

journal homepage: www.keaipublishing.com/en/journals/deepre/

Full length article

Influence of initial stress difference on the hard rock fracture mechanism under stepwise unloading during large high-stress underground powerhouse layered excavation

Liangjie Gu [a,*], Cong Xie [a], Yan Zhang [a], Wenjing Niu [b], Yaohui Gao [c], Ru Lin [a], Jiaxing Huang [a]

[a] State Key Laboratory of Geohazard Prevention and Geoenvironment Protection, Chengdu University of Technology, Chengdu 610059, China
[b] School of Resources, Environment and Materials, Guangxi University, Nanning 530004, China
[c] Power China Huadong Engineering Corporation Limited, Hangzhou 310014, China

ARTICLE INFO

Keywords:
Initial stress difference
True triaxial test
Stepwise unloading
Acoustic emission
Damage accumulation
Failure mechanism

ABSTRACT

With the continuous advancement of deep resource exploitation and underground engineering construction, the mechanical behavior and failure mechanisms of hard rock under stepwise unloading during Layered excavation of high-stress underground powerhouses have become critical scientific issues constraining engineering safety. Taking Shuangjiangkou granite as the research object, true triaxial stepwise unloading tests were conducted to systematically investigate the effects of different initial stress differences on rock strength, deformation, brittleness, and macro–micro failure mechanisms. In addition, AE monitoring was employed to reveal the evolution of cumulative crack damage and sudden failure. The results show that, with increasing initial stress difference, the peak strength of rock exhibits a nonlinear increase. The macroscopic failure mode evolves from diffuse shear propagation to directional splitting failure, while the microscopic fracture morphology transitions from intergranular shear cracks to transgranular tensile cracks. During the unloading process, AE energy exhibits a two-stage characteristic of steady accumulation followed by a sudden surge. Under higher initial stress differences, the duration of the rapid AE energy growth stage is significantly shortened, indicating that energy is more likely to be concentrated and released abruptly, resulting in macroscopic instability. Moreover, the degree of sudden rock failure increases logarithmically with the initial stress difference, consistent with the evolution of the brittleness index. These findings provide theoretical support for elucidating the failure mechanisms of hard rock during staged excavation of high-stress underground powerhouses.

1. Introduction

With the rapid development of deep resource exploitation and underground engineering construction, the mechanical behavior and failure mechanisms of hard rock under high-stress conditions have become a fundamental scientific issue constraining engineering safety [1–10]. In underground projects represented by large-scale hydropower powerhouses, the rock mass undergoes a layered and staged excavation process, which essentially constitutes a dynamic evolution from an initial state of high stress difference, through stepwise unloading, to subsequent stress redistribution. During this process, the rock mass is subjected not only to a true triaxial stress state characterized by three-dimensional unequal principal stresses, but also to a distinctive stepwise unloading stress path induced by the staged nature of excavation. This combined effect further intensifies the complexity of rock failure and renders the system highly prone to chain-type brittle disasters (see Fig. 1), posing severe threats to construction safety and overall engineering stability [11,12].

To address the unloading issues during deep excavation processes, numerous studies have been conducted on the mechanical behavior of rock under unloading conditions [13–17]. Research has shown that, under unloading conditions, the strength of rock tends to increase, but the difficulty of failure decreases while the severity of fracture intensifies, with a significant increase in energy release [18–21]. Gu et al. [22] indicated that the crack development time in rock under true triaxial unloading stress paths is delayed compared to a constant stress state, with changes observed in both the direction and location of the cracks. This reveals the dynamic evolution mechanism of crack

* Corresponding author.
E-mail address: gulj@cdut.edu.cn (L. Gu).

https://doi.org/10.1016/j.deepre.2025.100227
Received 10 September 2025; Received in revised form 12 October 2025; Accepted 27 October 2025
Available online 28 October 2025

propagation direction and position in hard rock. It is worth noting that, the rock mechanics parameters derived from unloading stress paths align more closely with actual excavation conditions [23–27]. Additionally, some researchers have demonstrated that an increase in intermediate principal stress and a decrease in minimum principal stress lead to a shift in the failure mode of rock from shear to tensile splitting [28–33].

The fracture mode and strength of rock are highly dependent on the stress path and initial stress state. Traditional true triaxial tests generally adopt conventional loading or single-stage unloading methods. While these experiments have revealed the influence of factors such as intermediate principal stress and unloading stress path, limitations exist in simulating the true mechanical environment of layered excavation in large underground powerhouses, resulting in discrepancies between experimental results and actual field conditions. Currently, with the burial depth of hydropower underground powerhouses and deep mining tunnels exceeding 500 m, statistical analysis shows that, in specific deep environments, gravitational stress is lower than the maximum horizontal principal stress, resulting in a small difference between the initial intermediate principal stress (σ_2^0) and the maximum principal stress (σ_3^0), while the difference with the minimum principal stress is larger [34–40]. Moreover, as the burial depth increases, the difference between the σ_2^0 and σ_3^0 gradually increases, showing a clear characteristic of high initial stress difference (see Fig. 2). However, systematic studies on the rock damage accumulation effects and fracture stage evolution under true triaxial stepwise unloading with high initial stress differences remain lacking.

Therefore, this study employed a true triaxial test system, complemented by acoustic emission monitoring and electron microscopy scanning equipment, to conduct true triaxial stepwise unloading experiments under different initial stress difference conditions. The research revealed the significant influence of initial stress difference and stepwise unloading on the fracture mode of hard rock, providing fundamental scientific basis and theoretical support for the safe construction of deep underground engineering projects.

2. Experimental design

2.1. Sample preparation and testing equipment

The rock samples were obtained from large, intact rock masses in the diversion tunnel of the underground powerhouse at the Shuangjiangkou Hydropower Station, Sichuan, China. The samples are granite with a medium-coarse-grained hypidiomorphic granular texture, where mineral grains are distributed in a uniform interlocking pattern without obvious orientation. Additionally, the interfaces between the mineral grains are clear, and there is no large-scale continuous aggregation of

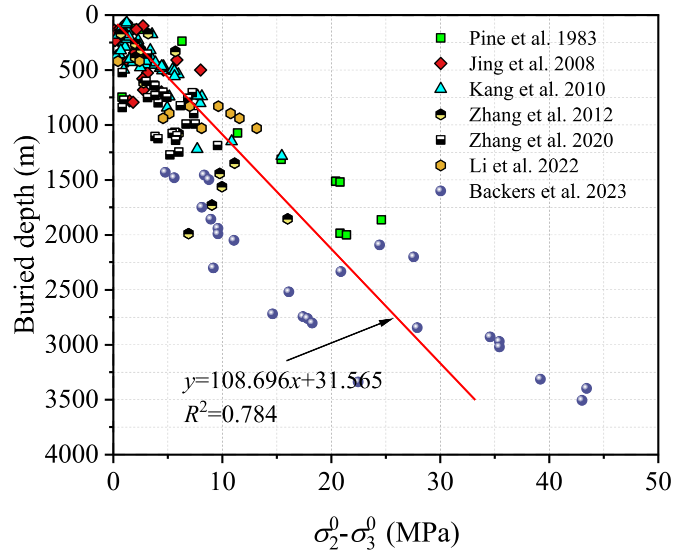

Fig. 2. Statistical results of initial stress difference and buried depth [33–39].

minerals. According to the standards set by the International Society for Rock Mechanics and Rock Engineering (ISRM), these field-collected rock pieces were cut and polished into rectangular standard specimens with dimensions of 50 mm × 50 mm × 100 mm. The specific processing accuracy requirements were as follows: edge length tolerance of ±0.1 mm, perpendicularity tolerance of adjacent faces of ±0.25°, and flatness tolerance of relative end faces of ±0.02 mm (see Fig. 3). To minimize experimental result dispersion, rock samples were selected based on longitudinal wave velocities measured using an ultrasonic velocity meter, with wave speeds between 3750–3850 m/s. Additionally, mineral composition analysis revealed that the rock primarily consists of quartz (32%), potassium feldspar (17%), plagioclase (36%), mica (12%), and other substances (3%). Due to the high quartz content and its brittle, hard texture, the granite exhibits a material basis for brittle failure. The Shuangjiangkou granite exhibits an uniaxial compression strength of approximately 140 MPa, and under conventional triaxial compression, its cohesion and internal friction angle are about 30 MPa and 43°, respectively.

The high-pressure servo-controlled true triaxial testing machine used in this study consists of a true triaxial loading system, an LVDT deformation measurement system, an acoustic emission system, and a video capture system (see Fig. 3). The machine is capable of independent loading and unloading along the X, Y, and Z axes, with a vertical maximum loading capacity of 5000 kN and a horizontal maximum

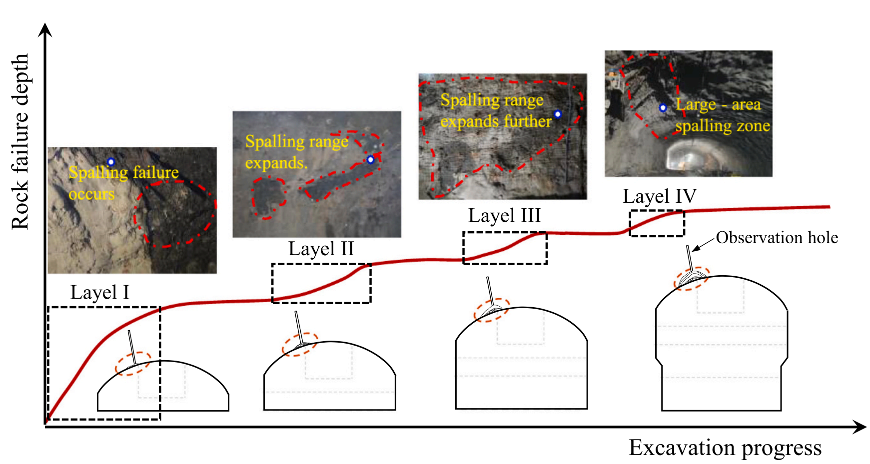

Fig. 1. Chain-type brittle failure process under layered excavation of the large underground powerhouse at Baihetan [11,12].

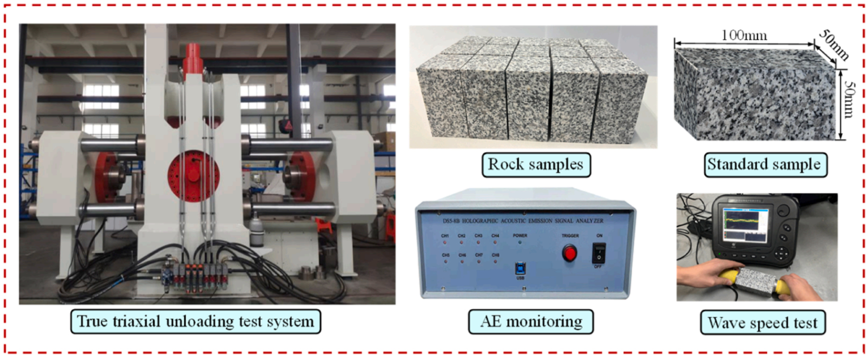

Fig. 3. True triaxial testing system and Shuangjiangkou granite specimen.

loading capacity of 3000 kN. The maximum stroke is 100 mm, with stress-strain control accuracy of ±0.5% F.S, and it supports long-duration steady-pressure loading. During the testing process, a DS5 series full-information acoustic emission (AE) signal analyzer was used to collect AE signals. Four Nano30-type AE sensors were symmetrically arranged on the four side faces of the specimen perpendicular to the maximum principal stress direction. The centers of the sensors were 25 mm away from both the upper and lower end faces of the specimen, and the distance between adjacent sensors was 50 mm. Petroleum jelly was used as a coupling agent between the sensors and the specimen surface to reduce signal attenuation. The AE signal trigger threshold was set to 40 dB to filter out invalid signals; the sampling frequency was set to 1 MHz, the preamplifier gain to 40 dB, and the signal threshold to 200 μV. Meanwhile, the pencil lead break test was conducted to verify the response consistency of the sensors, ensuring that all collected AE signals originated from microcrack activities inside the rock rather than equipment or environmental interference. After the test, scanning electron microscopy (SEM) was conducted on the fracture surface of the rock to obtain microscopic failure characteristics.

2.2. Experimental scheme and stress path design

To investigate the influence of different initial stress differences on rock fracture under true triaxial stepwise unloading stress paths, four initial stress difference values were selected: 0, 10, 40, and 90 MPa. The chosen stress path was defined by σ_1 loading, σ_2 remaining constant, and σ_3 unloading, as this condition most readily induces surrounding rock failure during underground excavation [21]. Therefore, this stress path more accurately represents the failure mechanisms of surrounding rock in deep hard rock excavations.

The experimental procedure consisted of two stages (see Fig. 4):

Initial stress loading stage: Confining pressure was first applied with $\sigma_1 = \sigma_2 = \sigma_3$. The three principal stresses were simultaneously increased to the target value of σ_3 at a rate of 0.25 MPa/s, after which σ_3 was held constant. Subsequently, both the maximum principal stress σ_1 and σ_2 were increased simultaneously at the same rate until σ_2 reached the predetermined value, which was then held constant. Finally, σ_1 was individually increased at 0.25 MPa/s. When σ_1 reached 85% of the rock's peak strength, it was maintained constant.

Stepwise unloading stage: During this stage, σ_2 remained constant, while σ_1 and σ_3 were respectively increased and decreased at a rate of 0.25 MPa/s. Each adjustment was carried out in increments of 1 MPa. After each adjustment, the stress state was maintained for 3–5 min until stabilization, where stabilization was defined by two criteria: (1) the fluctuation range of σ_1, σ_2, and σ_3 was $\leq 0.5\%$ F.S; (2) the deformation rate in all three principal stress directions was ≤ 0.001 mm/min. This dual-criterion ensured complete stress redistribution within the rock before proceeding to the next unloading step.

It is noteworthy that, during the true triaxial stepwise unloading tests, the initial maximum principal stress was set to 85% of the peak

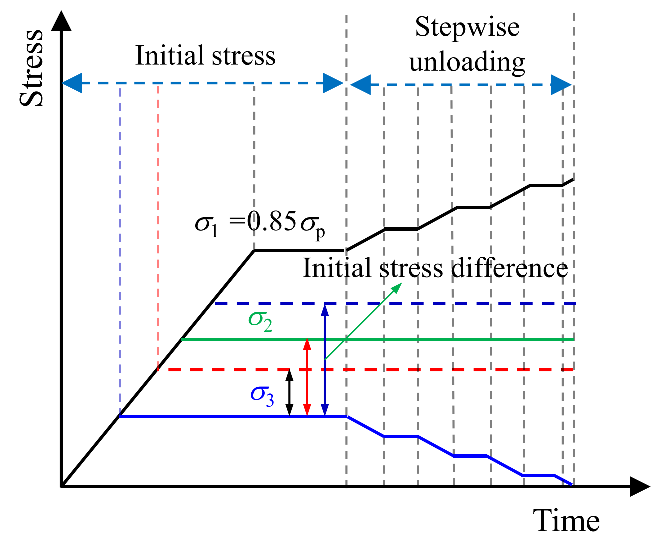

Fig. 4. Schematic diagram of the stress path during true triaxial stepwise unloading stress paths with different initial stress differences.

strength in order to avoid damage caused by the initial stress level. To determine the appropriate initial stress level for the true triaxial stepwise unloading tests, a preliminary true triaxial loading test was first conducted at the same loading rate as the formal tests (the loading rates of σ_1, σ_2, and σ_3 were all 0.25 MPa/s) to obtain the peak strength, and the test results are presented in Table 1.

3. Basic mechanical properties

The mechanical response of hard rock essentially involves a chain process of strength bearing, deformation evolution, and subsequent brittle instability under stress. Thus, this section analyzes the effects of initial stress difference on the strength, deformation, and brittleness of

Table 1
Results of true triaxial compression tests on Shuangjiangkou granite under different initial stress differences.

Test type	σ_3^0 (MPa)	σ_2^0 (MPa)	$\sigma_2^0 - \sigma_3^0$ (MPa)	σ_p (MPa)
Conventional triaxial compression	10	10	0	180.1
True triaxial compression	10	20	10	220.5
True triaxial compression	10	50	40	251.2
True triaxial compression	10	100	90	297.6

Shuangjiangkou granite, and reveals its regulatory mechanism under true triaxial stepwise unloading.

3.1. Strength difference

Fig. 5 presents the strength of Shuangjiangkou granite under true triaxial stepwise unloading stress paths with different initial stress differences. When the initial stress difference was 0 MPa, the peak strength was 161.03 MPa. At an initial stress difference of 10 MPa, the peak strength increased to 195.41 MPa, representing a gain of 34.38 MPa compared with 0 MPa. With an initial stress difference of 40 MPa, the peak strength rose to 222.02 MPa, an increase of 26.61 MPa relative to 10 MPa. When the initial stress difference reached 90 MPa, the peak strength attained 263.04 MPa, showing an increment of 41.02 MPa compared with 40 MPa.

These results indicate that the specimen strength exhibits a nonlinear growth trend with increasing initial stress difference. The most pronounced increase occurs between 0–10 MPa, reflecting the higher sensitivity of internal microcracks to stress changes at low initial stress differences. The strength increment slows between 10–40 MPa but rises again from 40 to 90 MPa, likely due to rapid energy accumulation under high initial stress differences, which concentrates macroscopic fracture pathways. Furthermore, the relationship between peak strength and initial stress difference can be well described by an exponential function, with a fitting coefficient of determination R^2= 0.95, demonstrating that the fitting curve captures the nonlinear evolution of strength with high accuracy.

3.2. Deformation difference

The increase in peak strength caused by the rise in initial stress difference essentially reflects the enhanced intergranular interlocking effect within the rock. This change in load-bearing capacity directly alters the distribution ratio of stress among the three principal stress directions, thereby leading to significant differences in the evolution of deformation along the σ_1, σ_2, and σ_3 directions, which is specifically manifested as the enhancement of deformation anisotropy. Fig. 6 presents the stress-strain curves of Shuangjiangkou granite under true triaxial stepwise unloading stress paths with different initial stress differences. It can be observed that under different stress difference, deformation along the maximum principal stress direction (ε_1) always exhibits contraction behavior, while deformation along the minimum principal stress direction (ε_3) shows an dilation. However, the deformation along the intermediate principal stress direction (ε_2) exhibits significant variation. As the initial stress difference increases, the deformation along the intermediate principal stress direction transitions from dilation to contraction (see Fig. 6b-d). Moreover, when the $\sigma_2^0 - \sigma_3^0 = 0$ MPa, the deformations along the intermediate and minimum principal stress directions are similar. As the stress difference increases, the strains along the intermediate and minimum principal stress directions gradually diverge, with the difference in deformation between these directions progressively increasing. This indicates that the initial stress difference not only constrains the applied stress on the rock but also imposes constraints on its deformation, significantly altering the deformation evolution along the intermediate and minimum principal stress directions, thereby influencing the development direction of rock fracture.

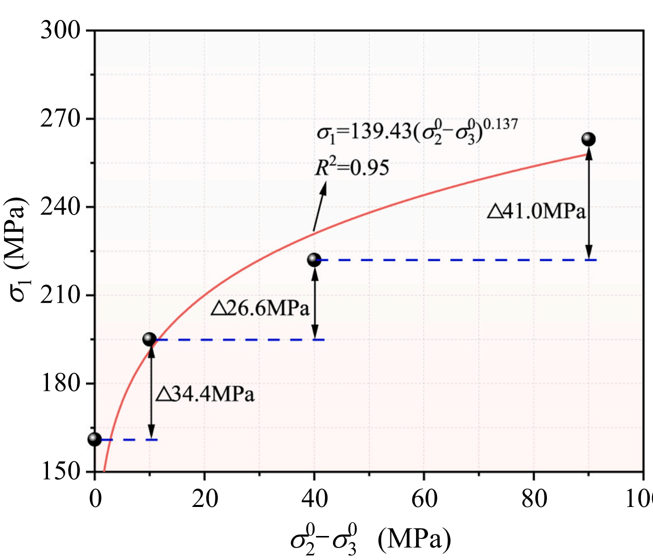

Fig. 5. Strength characteristics of Shuangjiangkou granite under true triaxial stepwise unloading stress paths with different initial stress differences.

Deformation is caused by differences in stress adjustment, so the ultimate strain and ultimate stress difference at rock failure under different stress differences during true triaxial stepwise unloading were analyzed. As shown in Fig. 7, with increasing initial stress difference, ε_1 decreases linearly, while ε_2 and ε_3 increase linearly. This suggests that, during true triaxial stepwise unloading, the increase in initial stress difference restricts the development of deformation in all three principal stress directions, causing the deformation along the intermediate principal stress direction to shift from dilation to contraction. This affects the differential development of deformation along the intermediate and minimum principal stress directions, ultimately leading to variations in the final failure modes.

To quantitatively measure the degree of deviation between the strain directions of the intermediate and minimum principal stresses, a deformation difference coefficient λ was defined, as expressed in Eq. (1):

$$\lambda = \frac{\varepsilon_3^f - \varepsilon_2^f}{\varepsilon_3^f} \tag{1}$$

As shown in Fig. 8, during the true triaxial stepwise unloading process, the deformation difference coefficient of the rock increases progressively with the initial stress difference and can be well fitted using a negative exponential function. This observation reveals the mechanism by which increasing initial stress differences promote the evolution of deformation anisotropy.

3.3. Brittleness difference

An increase in initial stress difference expands the deformation difference between the σ_2 and σ_3 directions. This uneven deformation causes cracks inside the rock to no longer propagate uniformly; instead, the concentrate toward the σ_3 direction, which accelerates the directional initiation and propagation of microcracks and reduces the buffer space for crack propagation, ultimately manifesting as a change in rock brittleness. To compare the brittleness characteristics of Shuangjiangkou granite under true triaxial stepwise unloading stress paths with different initial stress differences, the brittleness index (abbreviated as B_{TTS}), calculated from the stress–strain curves, was employed for quantitative description [41]. The specific formula is provided in Eq. (2):

$$B_{TTS} = \frac{K_1 - K_3}{K_1 - K_2} \cdot \frac{M_1 - K_1}{M_1} \tag{2}$$

where K_1, K_2, K_3, and M_1 represent the deformation moduli of the rock corresponding to σ_1, σ_2 and σ_3 before the peak strength, and the deformation modulus corresponding to σ_1 after the peak strength, respectively. Since the post-peak stage does not exist under the unloading stress path, Eq. (2) was modified to Eqs. (3) and (4):

$$B_{TLU} = \frac{K_1 - K_3}{K_1 - K_2} \tag{3}$$

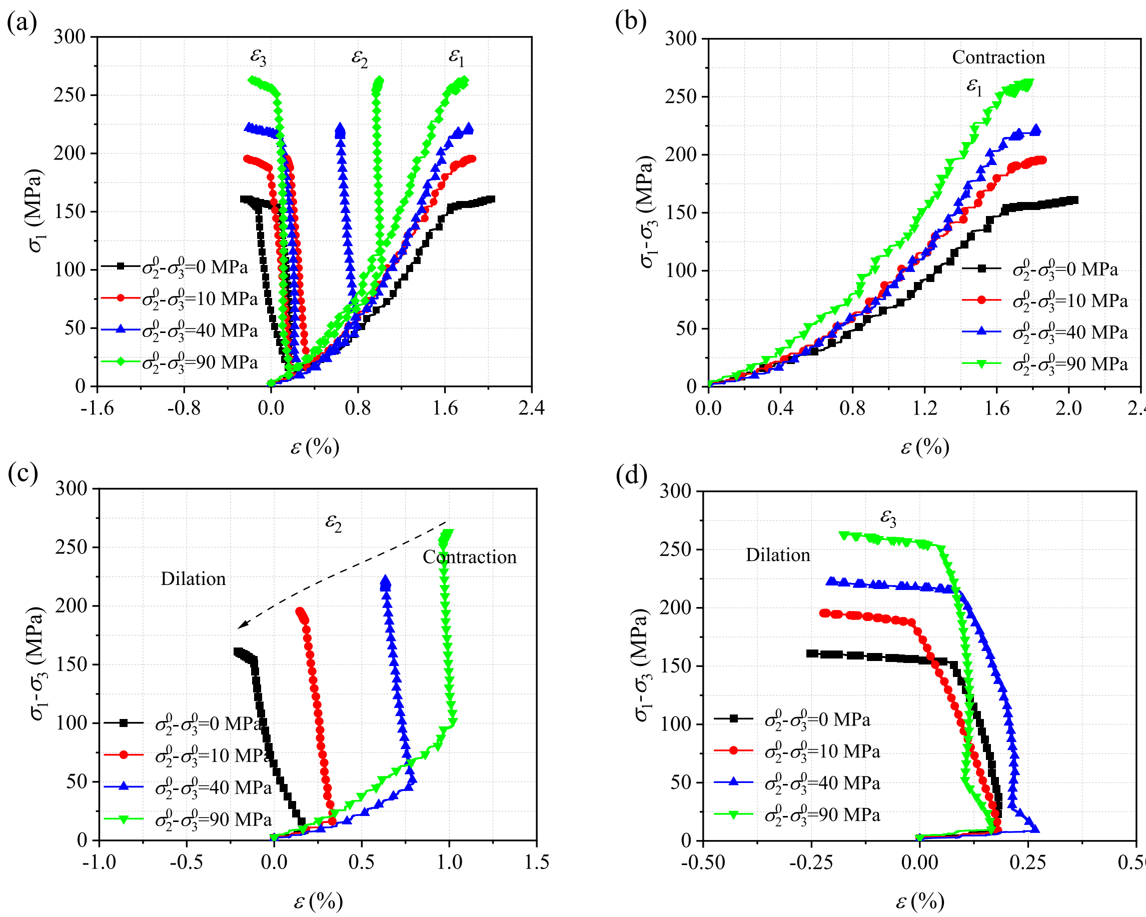

Fig. 6. Stress-strain curves of Shuangjiangkou granite under true triaxial stepwise unloading stress paths with different initial stress differences: (a) stress-strain curves in three directions; (b) stress-strain curves in the σ_1 direction; (c) stress-strain curves in the σ_2 direction; (d) stress-strain curves in the σ_3 direction.

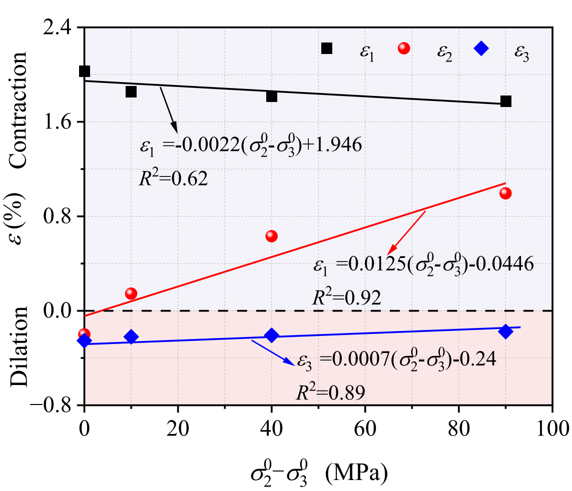

Fig. 7. Deformation anisotropy in Shuangjiangkou granite under true triaxial stepwise unloading stress paths with different initial stress differences.

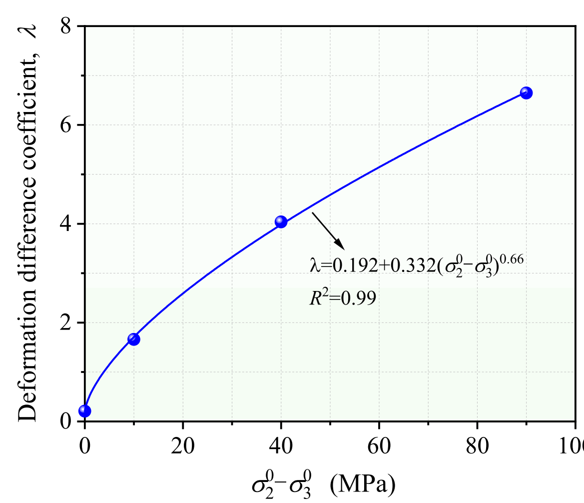

Fig. 8. Deformation difference coefficient of Shuangjiangkou granite under true triaxial stepwise unloading stress paths with different initial stress differences.

$$K_i = \frac{(\sigma_1^f - \sigma_3^f) - (\sigma_1^0 - \sigma_3^0)}{\varepsilon_i^f - \varepsilon_i^0} \tag{4}$$

where B_{TLU} denotes the brittleness index under stepwise unloading; $i = 1$, 2, and 3 correspond to the three principal stress directions. The superscript 0 represents the stress and strain values at the initial point, while f denotes the stress and strain values at rock failure. A smaller B_{TLU} value indicates greater brittleness of the rock.

As shown in Fig. 9, the brittleness index decreases progressively with increasing initial stress difference, indicating that the rock becomes increasingly brittle. However, the rate of brittleness enhancement gradually declines. This phenomenon essentially reflects the regulatory effect of the initial stress difference on the evolution of microcracks within the rock. At low stress differences, a large number of microcracks

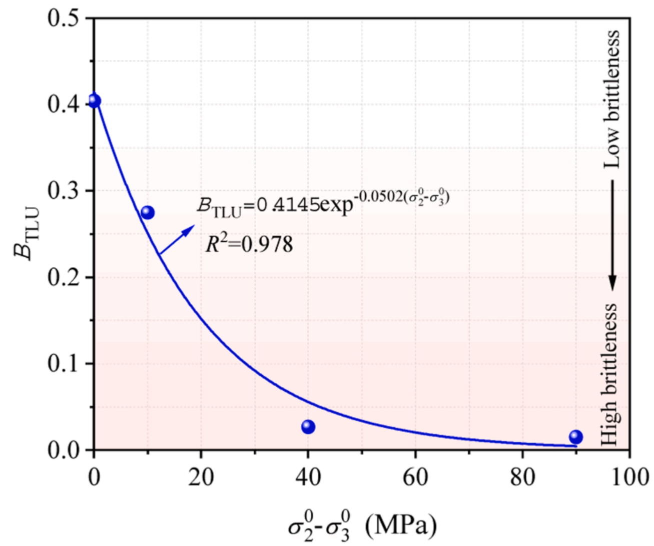

Fig. 9. Relationship between brittleness and initial stress difference of Shuangjiangkou granite under true triaxial stepwise unloading stress path.

with dispersed propagation directions exist, and a slight increase in initial stress difference rapidly promotes the directional propagation along the maximum principal stress and accelerates the coalescence, leading to a significant increase in brittleness. In contrast, once the stress difference exceeds a certain threshold, the propagation direction of microcracks becomes stabilized, and the number of activatable microcracks decreases. Consequently, additional stress differences have limited impact on the crack propagation mode, resulting in a diminishing marginal effect on brittleness enhancement and a gradual reduction in the growth rate. This trend can be well fitted by a power function, as expressed in Eq. (5):

$$B_{TLU} = 0.4145\exp^{-0.0502(\sigma_2^0-\sigma_3^0)} \quad (5)$$

4. Analysis of macroscopic and microscopic failure modes and mechanisms

4.1. Disparities in macroscopic and microscopic failure modes

The macroscopic failure mode is an external manifestation of the internal stress state and microcrack evolution of rock, and its failure angle shows a significant regular change with the increase of initial stress difference (see Figs. 10 and 11). When the initial stress difference is 0 MPa, rock cracks develop randomly along the directions of the intermediate and minimum principal stress, forming a large number of interlaced fine curved cracks, with a macroscopic failure angle of 64.5°, which generally exhibits the characteristics of diffuse shear failure. As the initial stress difference increases to 10 and 40 MPa, the cracks gradually concentrate and propagate parallel to the direction of the intermediate principal stress and along the direction of the minimum principal stress, and the failure angle rises to 72.3° and 80.3°, respectively; splitting characteristics begin to be integrated into the shear-dominated failure mode. When the initial stress difference reaches 90 MPa, the directionality of cracks is further enhanced, forming a single and straight macroscopic through-going splitting surface, with the failure angle stabilizing at 84.5°, which completely transforms into directional splitting failure.

The essence of this evolution lies in the regulation of the initial stress difference on the internal stress constraint state of the rock. Under low initial stress differences (0–10 MPa), the constraint difference between

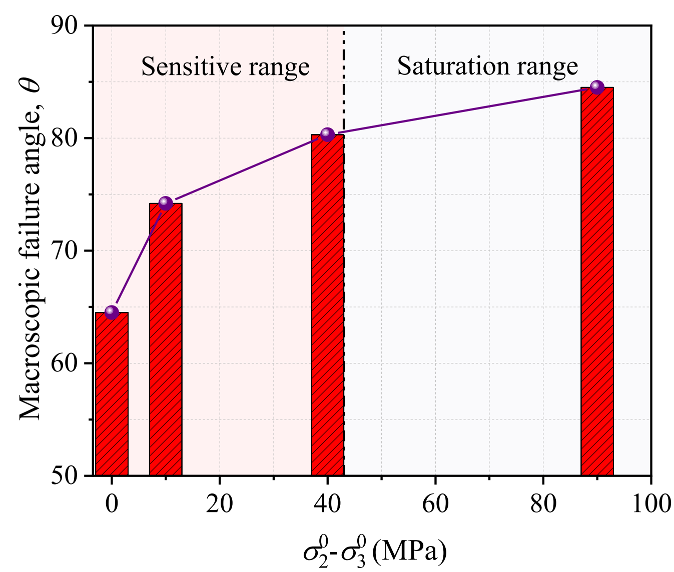

Fig. 11. Macroscopic failure angle of Shuangjiangkou granite under true triaxial stepwise unloading stress paths with different initial stress differences.

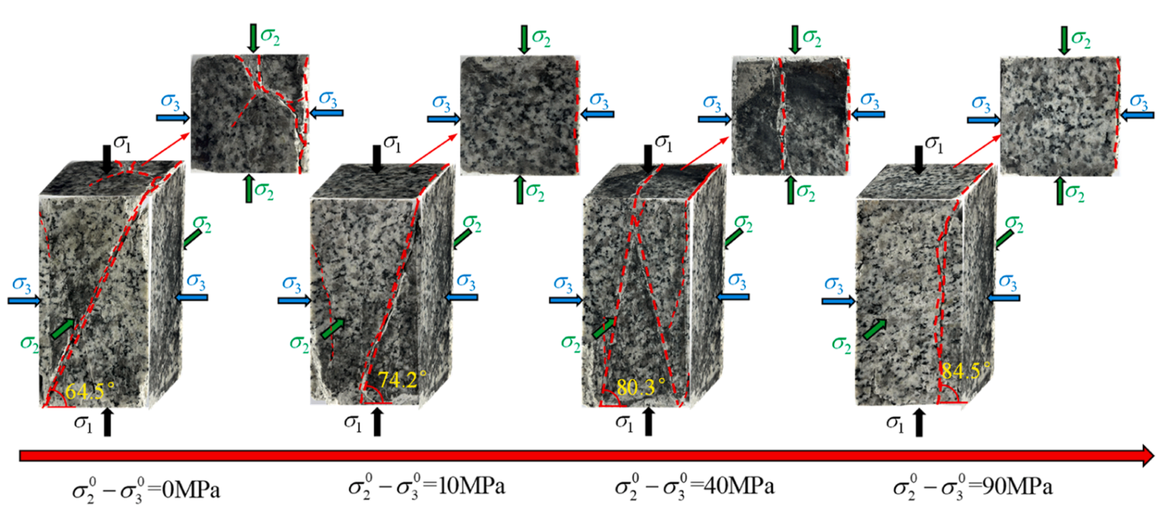

Fig. 10. Macroscopic failure modes of Shuangjiangkou granite under true triaxial stepwise unloading stress paths with different initial stress differences: (a) $\sigma_2^0-\sigma_3^0=0$ MPa; (b) $\sigma_2^0-\sigma_3^0=10$ MPa; (c) $\sigma_2^0-\sigma_3^0=40$ MPa; (d) $\sigma_2^0-\sigma_3^0=90$ MPa.

the intermediate and the minimum principal stress is small, the stress gradient in the three principal stress directions is gentle, and microcracks have no obvious preferential propagation direction, only propagating randomly along weak regions such as grain boundaries, eventually forming a diffusely distributed shear surface. Under high initial stress differences (40–90 MPa), the constraint difference between intermediate and the minimum principal stress increases significantly, and the lateral constraint in the direction of the minimum principal stress weakens sharply, leading to a prominent tensile stress concentration effect in this direction; microcracks preferentially propagate directionally along the direction dominated by tensile stress, and finally converge into a macroscopic splitting surface.

Notably, the influence of the initial stress difference on the failure angle has a "sensitive zone" (0–40 MPa) and a "saturation zone" (40–90 MPa). In the sensitive zone, for every 10 MPa increase in stress difference, the failure angle increases by an average of 3.95°; while in the saturation zone, even with a 50 MPa increase in stress difference, the failure angle only increases by 4.2°. This means that under high initial stress differences, the direction of the fracture surface tends to be basically stable. For large-scale engineering projects in such high-pressure environments, the fracture angle can be regarded as a relatively stable parameter, which enables more accurate estimation of the depth and extent of brittle failure in hard rock and facilitates the design of support systems with optimal bolt lengths and installation angles.

To investigate the influence of true triaxial stepwise unloading on the microscopic failure characteristics of Shuangjiangkou granite under different initial stress differences, scanning electron microscopy (SEM) was employed to observe the fracture surface morphology of the specimens. First, for each rock sample failed under a specific initial stress difference, the main fracture surface and typical failure regions were located through macroscopic observation. Subsequently, 2–3 representative sub-regions were selected near the main fracture surface, with priority given to positions that could reflect the macroscopic failure trend, while avoiding edge fragmented areas or non-dominant failure regions. Meanwhile, the magnification of the SEM was adjusted as needed to capture the key microscopic features of the rock samples. The SEM observation results further revealed the microscopic mechanism underlying the macroscopic failure modes. An increase in the initial stress difference drives the transition of microscopic fracture morphology from being dominated by intergranular shear to being dominated by transgranular tensile (see Fig. 12). When the initial stress difference is 0 MPa and 10 MPa, obvious shear scratches and intergranular separation characteristics are visible on the fracture surface; microcracks propagate mainly along the grain boundaries of minerals such as quartz and feldspar, forming uneven serrated fracture surfaces. This is consistent with the microscopic origin of macroscopic shear failure—since the intergranular bonding strength is lower than the intragranular strength, shear stress under low initial stress differences preferentially causes grain boundary separation, resulting in intergranular shear cracks.

When the initial stress difference increases to 40 and 90 MPa, the fracture surface becomes flat and smooth; instead of propagating along grain boundaries, microcracks directly traverse quartz grains to form transgranular cracks, accompanied by a large number of tensile-dominated stepped fracture features. This is because the tensile stress concentration under high initial stress differences exceeds the intragranular bonding strength, forcing microcracks to propagate transgranularly and further forming macroscopic directional splitting surfaces. It should be specifically noted that these stepped cracks are not shear cracks but secondary features dominated by tension. The propagation paths exhibit transgranular characteristics, directly traversing mineral grains such as quartz and feldspar; moreover, there are no obvious scratches formed by shear slip at the crack steps, but instead, cleavage planes characteristic of tensile fracture are observable. This is highly consistent with the formation mechanism of transgranular tensile cracks, reflecting that the microscopic failure mode of the rock is dominated by tensile failure at this point.

4.2. Microcrack evolution process based on acoustic emission

AE technology enables real-time acquisition of information regarding the initiation, propagation, and coalescence of microcracks in rock under stress. Regardless of the magnitude of the initial stress difference, the AE evolution process of Shuangjiangkou granite under true triaxial stepwise unloading exhibits a consistent two-stage characteristic, which corresponds to different stages of internal microcrack development in the rock (see Fig. 13). The early stage of stepwise unloading is the steady accumulation stage (Stage a-b). During this period, the rock mainly undergoes elastic deformation, with no significant propagation of pre-existing internal microcracks; only a small number of microfractures occur locally due to stress concentration. The AE energy rate remains at a low level, and the cumulative AE energy curve shows an approximately linear increase, indicating that no macroscopic fracturing occurs in the rock and internal damage is in a state of slow accumulation. As the number of unloading steps increases, the process enters the rapid surge stage (Stage b-c): internal stress redistribution in the rock intensifies, isolated microcracks continuously initiate, propagate, and coalesce, the AE energy rate rises sharply, and the cumulative AE energy curve exhibits a steep exponential increase. When the specimen undergoes complete macroscopic failure (Point c), the cumulative AE energy reaches its peak. This is attributed to the sudden release of a large amount of internal energy caused by the formation of macroscopic through-going cracks, which is directly manifested as a sharp surge in AE signals.

Although the AE evolution follows the two-stage law, the initial stress difference exerts a differential regulatory effect on the key characteristics of each stage. In terms of the duration of the rapid surge stage: when the initial stress difference is 0 MPa, the duration of this stage is approximately 144 s; as the initial stress difference increases to 10 and 40 MPa, the duration shortens to 133 and 87 s, respectively; when the initial stress difference reaches 90 MPa, the duration is only 59 s (see Fig. 14). This indicates that under high initial stress differences, the internal stress concentration in the rock is more significant, the rate of microcrack propagation and coalescence accelerates, and the process from damage accumulation to macroscopic instability is greatly compressed. In terms of the peak cumulative AE energy at failure: when the initial stress difference is 0 MPa, the peak value is approximately 0.76×10^4 ms·mV; when the initial stress difference increases to 90 MPa, the peak value reaches 5.89×10^4 ms·mV, an increase of 675% compared with the condition of 0 MPa (see Fig. 14). This reflects that under high initial stress differences, the rock accumulates more internal energy during the unloading process, and the intensity of sudden energy release during failure is more severe, which is consistent with the high-energy failure characteristics of hard rock under high-stress conditions.

5. Discussion

5.1. Control effect of initial stress difference on fracture mechanism

To elucidate the differential fracture mechanisms of hard rock under varying initial stress differences, cast thin sections of Shuangjiangkou granite samples were taken from specimens subjected to stepwise unloading under different initial stress differences. The grain characteristics and crack morphologies inside the samples, along with the relationships to the principal stresses, are shown in Fig. 15. When the initial stress difference is 0 MPa, cracks are widely dispersed on all three

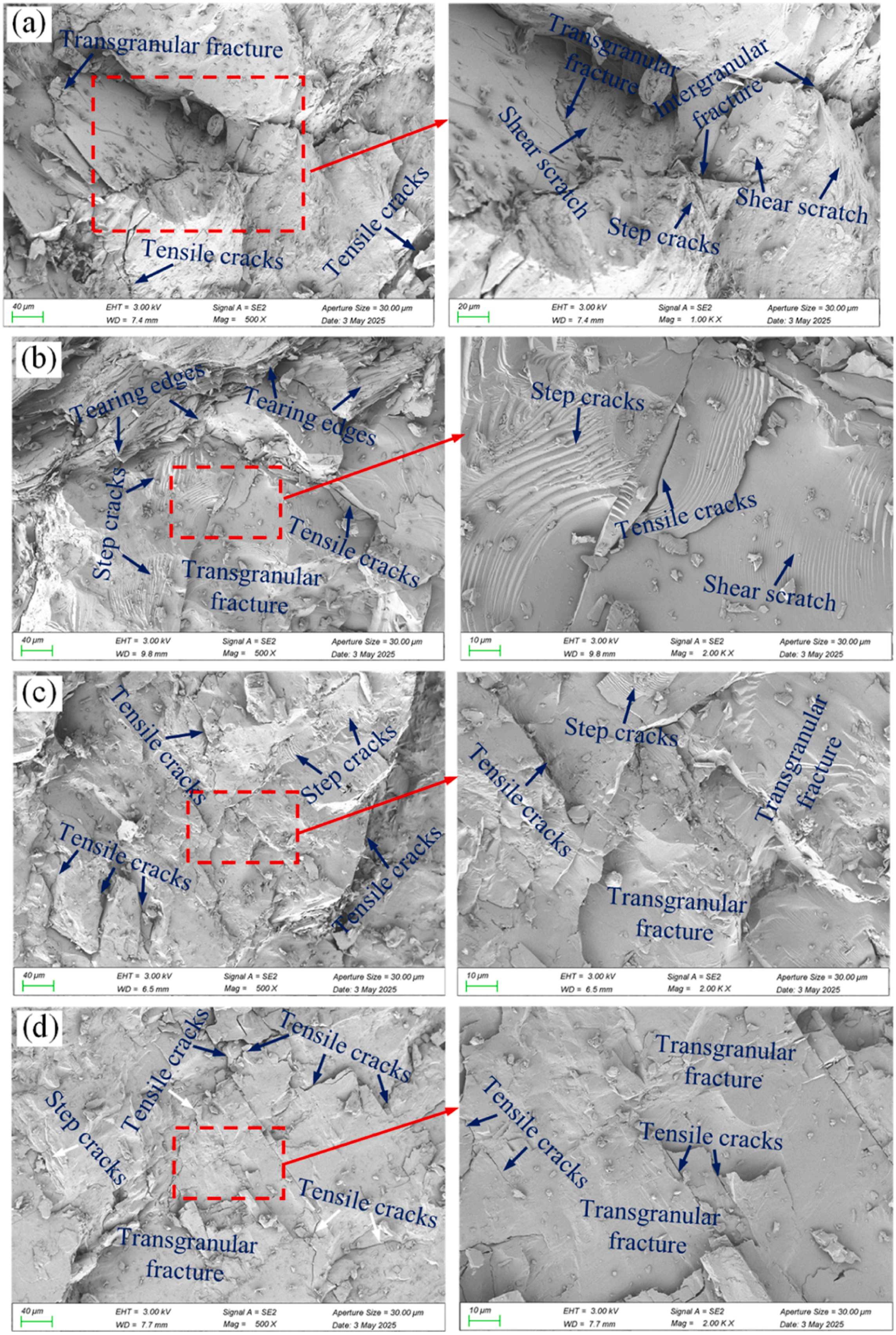

Fig. 12. Microscopic failure modes of Shuangjiangkou granite under true triaxial stepwise unloading stress paths with different initial stress differences: (a) $\sigma_2^0 - \sigma_3^0 = 0$ MPa; (b) $\sigma_2^0 - \sigma_3^0 = 10$ MPa; (c) $\sigma_2^0 - \sigma_3^0 = 40$ MPa; (d) $\sigma_2^0 - \sigma_3^0 = 90$ MPa.

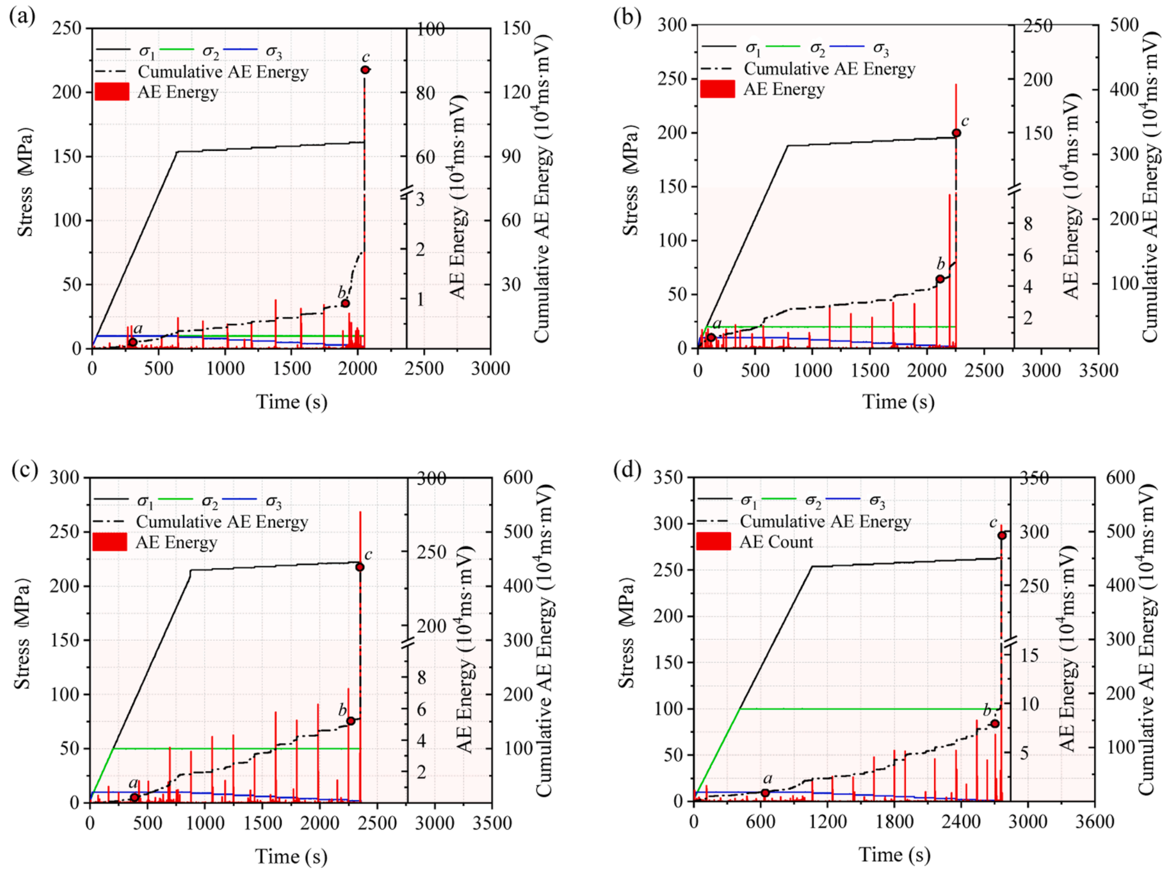

Fig. 13. AE evolution process of Shuangjiangkou granite under true triaxial stepwise unloading stress paths with different initial stress differences: (a) $\sigma_2^0 - \sigma_3^0 = 0$ MPa; (b) $\sigma_2^0 - \sigma_3^0 = 10$ MPa; (c) $\sigma_2^0 - \sigma_3^0 = 40$ MPa; (d) $\sigma_2^0 - \sigma_3^0 = 90$ MPa.

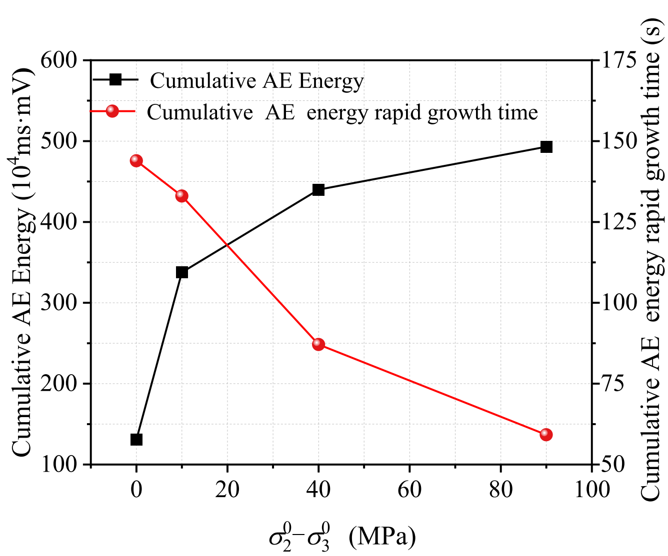

Fig. 14. Cumulative AE energy and rapid growth time of Shuangjiangkou granite under true triaxial stepwise unloading stress paths with different initial stress differences.

cross-sections, with weak orientation. The cracks show random relationships with the grain boundaries and cleavage planes, and the overall fracture pattern is characterized by uniform extension. However, when the initial stress difference increases to 90 MPa, the number of cracks decreases, and the cracks exhibit a clear control effect by the principal stresses on the cross-sections. On the σ_2—σ_3 plane, cracks tend to concentrate and extend along the σ_3 direction, demonstrating the expansion advantage resulting from lateral constraint insufficiency. On the σ_1—σ_3 plane, cracks form in a band-like distribution with strong directional alignment, with localized cleavage connectivity observed. On the σ_1—σ_2 plane, nearly no microcracks are generated, primarily due to the suppression of cracks in this direction by the initial stress difference.

Overall, as the initial stress difference increases, the crack distribution becomes more concentrated and exhibits more pronounced directionality. The failure mode transitions from a uniform, diffuse fracture pattern at low initial stress differences to a cleavage-dominated directional failure mechanism at high initial stress differences.

5.2. Influence of initial stress difference on the cumulative damage during true triaxial stepwise unloading

During true triaxial stepwise unloading, the internal damage of rock is not generated instantaneously, but rather exhibits a cumulative effect as stress is gradually released. Experimental results demonstrate that, in the early stage of unloading, Shuangjiangkou granite primarily undergoes an elastic response, with only a few pre-existing microcracks being activated due to stress concentration. At this stage, the AE energy rate remains low, and the cumulative AE energy curve shows an approximately linear growth. However, as the number of unloading steps increases, stress redistribution progressively promotes microcrack initiation and propagation. The cumulative AE energy enters an accelerated growth phase, reflecting a typical temporal evolution of damage characterized by steady accumulation followed by a sudden surge. This process is strongly influenced by the magnitude of the initial stress difference. Under low initial stress differences, damage evolves relatively slowly. Meanwhile, microcracks tend to expand in a diffuse

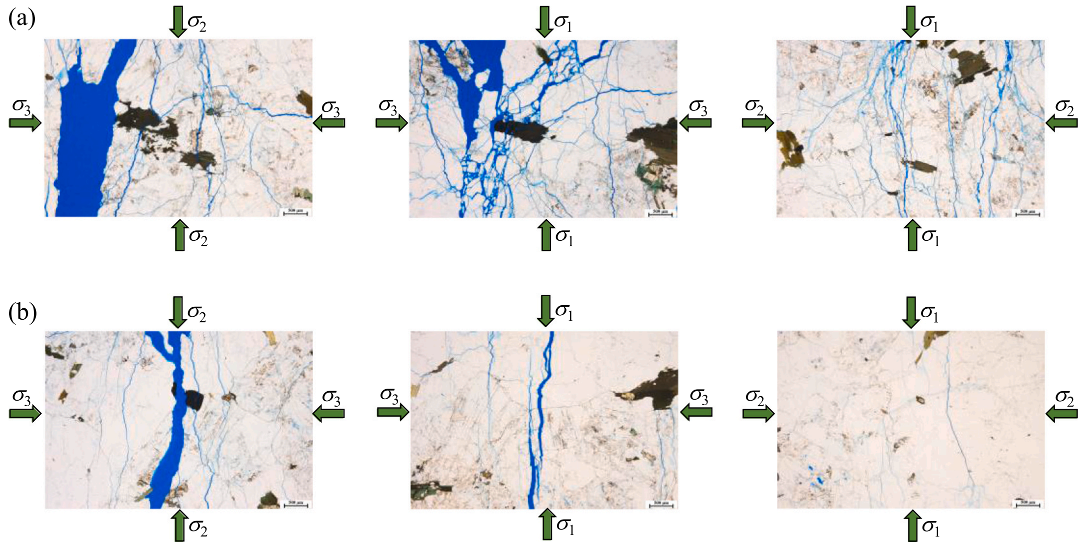

Fig. 15. Microcrack morphology of Shuangjiangkou granite under true triaxial stepwise unloading stress paths with different initial stress differences: (a) $\sigma_2^0 - \sigma_3^0 = 0$ MPa; (b) $\sigma_2^0 - \sigma_3^0 = 90$ MPa.

manner. In contrast, high initial stress differences lead to three distinct phenomena: first, internal energy accumulates rapidly; second, crack propagation accelerates significantly; third, the duration of the rapid increase in cumulative AE energy shortens. This indicates that damage is more likely to be concentrated and released abruptly within a short period, thereby inducing macroscopic failure.

To quantitatively evaluate the degree of abrupt, high-energy failure of rock during stepwise unloading under different initial stress differences, the variation of cumulative AE energy per unit time during the rapid-growth stage is defined as the index of sudden failure intensity, as expressed by Eq. (6):

$$S_F = \frac{U_c - U_b}{T_c - T_b} \tag{6}$$

where S_F denotes the rock sudden failure degree; U_b and T_b represent the cumulative AE energy and the corresponding time at the onset of the steady growth stage; while U_c and T_c correspond to the cumulative AE energy and the time at the rapid growth stage.

As illustrated in Fig. 16, the rock sudden failure degree increases with the initial stress difference, exhibiting a logarithmic growth trend similar to that observed for the brittleness index. This phenomenon reveals the coexistence of gradual and abrupt mechanisms in the damage

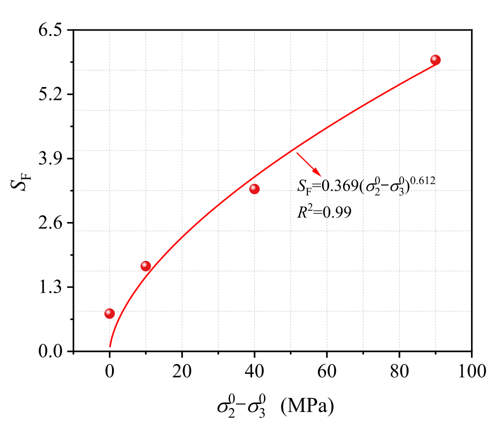

Fig. 16. Rock sudden failure degree of Shuangjiangkou granite under true triaxial stepwise unloading stress paths with different initial stress differences.

evolution of granite under true triaxial stepwise unloading. Specifically, during the initial stage, microcrack activation is primarily oriented and energy accumulates slowly, whereas in the pre-failure stage, the process is dominated by abrupt energy release and rapid crack coalescence. Ultimately, this results in a cross-scale evolutionary process from microscopic damage to macroscopic splitting failure.

5.3. Mechanism of initial stress difference-induced failure mode transition

The fundamental mechanical mechanism underlying the transition of the macroscopic failure mode from diffuse shear to directional splitting lies in the regulatory effect of the initial stress difference on the propagation direction and type of microcracks, which can be quantitatively analyzed based on the basic principles of fracture mechanics. According to linear elastic fracture mechanics, the response of a flattened elliptical crack inside the rock under far-field stress can be characterized by the stress intensity factor at its tip. For a crack oriented at an arbitrary angle to the principal stress directions, the classical calculation formulas for the Mode I (opening mode) and Mode II (sliding mode) stress intensity factors (K_I and K_{II}) are as follows [42,43]:

$$K_I = \sigma\sqrt{\pi a}\cdot Y_I \tag{7}$$

$$K_{II} = \tau\sqrt{\pi a}\cdot Y_{II} \tag{8}$$

where σ is the normal stress acting on the crack surface, τ is the shear stress acting on the crack surface, and Y_I and Y_{II} are correction coefficients related to crack shape, size, and sample geometry.

In true triaxial unloading tests, the stress state is more complex. Consider a crack whose normal is perpendicular to the σ_3 direction (one of the most dangerous potential cracks). The effective normal stress and shear stress acting on this crack surface are the combined result of the three principal stresses. During the unloading process, the decrease in σ_3 directly reduces the normal compressive stress acting on the crack surface and may even convert it into effective tensile stress, thereby significantly increasing the K_I that drives the tensile propagation of the crack. Maintaining a constant high σ_2 value exerts a strong constraint on cracks parallel to the σ_1—σ_2 plane. This constraint greatly inhibits the development of K_{II}, which drives the shear slip of the crack.

Therefore, an increase in the initial stress difference enhances the propagation advantage of cracks parallel to the σ_2—σ_3 plane (mainly controlled by K_I) while suppressing cracks controlled by K_{II}. According to the maximum circumferential stress criterion, the crack will propagate in the direction that makes K_{II} zero, and finally stabilize in the direction perpendicular to the minimum principal stress. When K_I at the crack tip reaches the fracture toughness of the material, the crack will undergo unstable propagation.

This mechanism explains that under high initial stress differences, K_I becomes the dominant driving force for propagation, resulting in a smooth, high-angle splitting surface macroscopically (a typical characteristic of Mode I fracture) and transgranular tensile cracks predominantly microscopically. In contrast, under low initial stress differences, both K_I and K_{II} make significant contributions to cracks with various orientations, leading to the formation of a complex mixed fracture network, which manifests as diffuse shear failure.

6. Conclusions

Based on true triaxial stepwise unloading tests, this study systematically investigated the strength, deformation, brittleness, and multi-scale failure mechanisms of hard rock under different initial stress differences. In addition, AE monitoring was employed to reveal the evolution process of cumulative damage and sudden failure. The main conclusions are as follows:

(1) With increasing initial stress difference, the peak strength of rock exhibits a nonlinear growth trend, with the enhancement being more pronounced at lower stress differences. Concurrently, the macroscopic failure mode gradually evolves from diffuse shear propagation to directional splitting failure, while the microscopic fracture morphology transitions from shear striations and intergranular cracks to predominantly transgranular tensile cracks.

(2) In the early stage of stepwise unloading, only a few microcracks are activated within the rock, and the cumulative AE energy increases slowly. As unloading progresses, crack propagation intensifies, AE events enter a rapid growth phase, and damage accumulates at an accelerated rate, eventually leading to macroscopic instability. Increasing initial stress difference shortens the duration of this rapid growth stage, indicating that higher initial stress differences promote concentrated energy release within shorter time intervals.

(3) The rock sudden failure degree increases with the initial stress difference, following a logarithmic growth trend consistent with the evolution of the brittleness index. This finding reveals the coupled mechanism in which macroscopic damage evolves from gradual accumulation to rapid macroscopic crack coalescence.

CRediT authorship contribution statement

Liangjie Gu: Writing – original draft, Validation, Methodology, Funding acquisition, Formal analysis, Data curation. **Cong Xie:** Writing – review & editing, Supervision, Conceptualization. **Yan Zhang:** Writing – review & editing, Methodology. **Wenjing Niu:** Writing – review & editing. **Yaohui Gao:** Writing – review & editing. **Ru Lin:** Writing – review & editing. **Jiaxing Huang:** Writing – review & editing.

Declaration of Competing Interest

The authors declare that they have no known competing financial interests or personal relationships that could have appeared to influence the work reported in this paper.

Acknowledgments

The authors gratefully acknowledge financial support from the National Natural Science Foundation of China (Grant No. 52409125), the Sichuan Province Science and Technology Support Program (Grant No. 2025ZNSFSC1370), and the State Key Laboratory of Geohazard Prevention and Geoenvironment Protection Independent Research Project (Grant No. SKLGP2024Z010). The authors would also like to thank the journal editors and anonymous reviewers for their valuable suggestions.

Data availability statement

All data included in this study are available upon reasonable request by contact with the corresponding author.

References

[1] X.T. Feng, C.X. Yang, R. Kong, et al., Excavation-induced deep hard rock fracturing: Methodology and applications, J. Rock Mech. Geotech. Eng. 14 (1) (2022) 1–34.
[2] C.L. Wang, B.B. He, X.L. Hou, et al., Stress–energy mechanism for rock failure evolution based on damage mechanics in hard rock, Rock Mech. Rock Eng. 53 (2020) 1021–1037.
[3] M.C. He, Q. Wang, Excavation compensation method and key technology for surrounding rock control, Eng. Geol. 307 (2022) 106784.
[4] S.F. Wang, X.B. Li, J.R. Yao, et al., Experimental investigation of rock breakage by a conical pick and its application to non-explosive mechanized mining in deep hard rock, Int. J. Rock Mech. Min. Sci. 122 (2019) 104063.
[5] G.Q. Chen, L.J. Gu, Q. Xu, et al., Shear properties of non-persistent coplanar fractured hard rocks under normal stress unloading, J. Rock Mech. Geotech. Eng. 17 (6) (2025) 3593–3608.
[6] L.J. Gu, X.T. Feng, R. Kong, et al., Effect of principal stress direction interchange on the failure characteristics of hard rock, Int. J. Rock Mech. Min. Sci. 164 (2023) 105365.
[7] L.J. Gu, J. Zhao, Y.Y. Zhou, et al., Effect of stress difference and microfabric on the strength of deep granite, Bull. Eng. Geol. Environ. 84 (2025) 127.
[8] W. Wang, Y.S. Pan, H.R. Zhao, et al., Electric charge induction monitoring of deformation and failure behavior of igneous rock: Laboratory test and field application, J. Rock Mech. Geotech. Eng. 18 (2) (2026) 861–886.
[9] W. Wang, L.K. Zhao, Y.S. Pan, et al., Evolution characteristics of an induced electric charge signal and identification method of charge for instability failure in loaded coal, J. Rock Mech. Geotech. Eng. 17 (7) (2025) 3973–3993.
[10] H. Xu, G. Wang, Q. Jiang, et al., Mechanical properties and dilatancy angle model of jointed hard rock under true triaxial cyclic loading and unloading, Int. J. Coal Sci. Technol. 12 (2025) 85.
[11] X.T. Feng, S.F. Pei, Q. Jiang, et al., Deep fracturing of the hard rock surrounding a large underground cavern subjected to high geostress: In situ observation and mechanism analysis, Rock Mech. Rock Eng. 50 (2017) 2155–2175.
[12] G.F. Liu, X.T. Feng, Q. Jiang, et al., In situ observation of spalling process of intact rock mass at large cavern excavation, Eng. Geol. 226 (2017) 52–69.
[13] C. Pan, C.Y. Liu, G.M. Zhao, et al., Fractal characteristics and energy evolution analysis of rocks under true triaxial unloading conditions, Fractal Fract. 8 (7) (2024) 387.
[14] X.F. Si, F.Q. Gong, Strength-weakening effect and shear-tension failure mode transformation mechanism of rockburst for fine-grained granite under triaxial unloading compression, Int. J. Rock Mech. Min. Sci. 131 (2020) 104347.
[15] C.Y. Liu, G.M. Zhao, W.S. Xu, et al., Experimental study on failure characteristics of single-sided unloading rock under different intermediate principal stress conditions, Int. J. Min. Sci. Technol. 33 (3) (2023) 275–287.
[16] Y. Zhao, J. Bi, C.L. Wang, et al., Effect of unloading rate on the mechanical behavior and fracture characteristics of sandstones under complex triaxial stress conditions, Rock Mech. Rock Eng. 54 (2021) 4851–4866.
[17] G.S. Su, L.H. Hu, X.T. Feng, et al., True triaxial experimental study of rockbursts induced by ramp and cyclic dynamic disturbances, Rock Mech. Rock Eng. 51 (2018) 1027–1045.
[18] X.B. Li, K. Du, D.Y. Li, True triaxial strength and failure modes of cubic rock specimens with unloading the minor principal stress, Rock Mech. Rock Eng. 48 (2015) 2185–2196.
[19] K. Du, M. Tao, X.B. Li, et al., Experimental study of slabbing and rockburst induced by true-triaxial unloading and local dynamic disturbance, Rock Mech. Rock Eng. 49 (2016) 3437–3453.
[20] F. Feng, S.J. Chen, Y.J. Wang, et al., Cracking mechanism and strength criteria evaluation of granite affected by intermediate principal stresses subjected to unloading stress state, Int. J. Rock Mech. Min. Sci. 143 (2021) 104783.
[21] L.J. Gu, X.T. Feng, R. Kong, et al., Excavation stress path induced fracturing mechanism of hard rock in deep tunnel, Rock Mech. Rock Eng. 56 (2023) 1779–1806.
[22] L.J. Gu, X.T. Feng, R. Kong, et al., Influence of excavation stress paths on failure feature of deep hard rocks, Acta Geotech. 19 (2024) 1107–1128.
[23] F. Trippetta, C. Collettini, P.G. Meredith, et al., Evolution of the elastic moduli of seismogenic Triassic Evaporites subjected to cyclic stressing, Tectonophysics 592 (2013) 67–79.
[24] C.H. Ren, J. Yu, S.Y. Liu, et al., A plastic strain-induced damage model of porous rock suitable for different stress paths, Rock Mech. Rock Eng. 55 (2022) 1887–1906.
[25] W.Q. Cai, H.H. Zhu, W.H. Liang, Three-dimensional tunnel face extrusion and reinforcement effects of underground excavations in deep rock masses, Int. J. Rock Mech. Min. Sci. 150 (2022) 104999.

[26] L.J. Gu, X.T. Feng, R. Kong, et al., Evolution of mechanical parameters of Shuangjiangkou granite under different loading cycles and stress paths, J. Rock Mech. Geotech. Eng. 16 (4) (2024) 1113–1126.
[27] Y. Xie, Z.F. Wang, P.Z. Pan, et al., Rock failure analysis spanning two magnitude scales incorporating micro-cracks adjacent to the dominant macro-fracture tip, Eng. Fail. Anal. 181 (2025) 109958.
[28] L.J. Gu, G.Q. Zhu, S. Yu, et al., Directional development mechanism of hard rock fracture under true triaxial stress: Insights from macroscopic and microscopic fracture perspectives, Eng. Fract. Mech. 319 (2025) 111000.
[29] H.P. Xie, J. Lu, C.B. Li, et al., Experimental study on the mechanical and failure behaviors of deep rock subjected to true triaxial stress: A review, Int. J. Min. Sci. Technol. 32 (5) (2022) 915–950.
[30] D. Gao, J. Peng, F.C.Y. Kwok, et al., Influence of intermediate principal stress on mechanical and failure properties of anisotropic sandstone, Rock Mech. Rock Eng. 57 (2024) 7795–7812.
[31] J. Zhao, X.T. Feng, X.W. Zhang, et al., Brittle-ductile transition and failure mechanism of Jinping marble under true triaxial compression, Eng. Geol. 232 (2018) 160–170.
[32] L.J. Gu, Y.Y. Zhou, Y.X. Xiao, et al., Effect of initial stress difference on hard rock fracture mechanism under true triaxial excavation unloading stress paths, Rock Mech. Rock Eng. 57 (2024) 10205–10227.
[33] K. Peng, R.Z. Lai, S. Luo, et al., Influence of axial stress on failure characteristics of deep arched hard rock roadway, Trans. Nonferrous Met. Soc. China 34 (12) (2024) 4032–4048.
[34] R.J. Pine, P. Ledingham, C.M. Merrifield, In-situ stress measurement in the Carnmenellis granite—II. Hydrofracture tests at Rosemanowes quarry to depths of 2000 m, Int. J. Rock Mech. Min. Sci. Geomech. Abstr. 20 (2) (1983) 63–72.
[35] F. Jing, Q. Sheng, Y.H. Zhang, et al., Statistical analysis of geostress distribution laws for different rocks, Rock Soil Mech. 29 (7) (2008) 1877–1883 (in Chinese).
[36] H. Kang, X. Zhang, L. Si, et al., In-situ stress measurements and stress distribution characteristics in underground coal mines in China, Eng. Geol. 116 (3–4) (2010) 333–345.
[37] C.Q. Zhang, X.T. Feng, H. Zhou, Estimation of in situ stress along deep tunnels buried in complex geological conditions, Int. J. Rock Mech. Min. Sci. 52 (2012) 139–162.
[38] P. Zhang, Z.P. Meng, S. Jiang, et al., Characteristics of in-situ stress distribution in Zhengzhuang Region, Southern Qinshui Basin, China and its stress path during depletion, Eng. Geol. 264 (2020) 105413.
[39] X.B. Li, J.Z. Chen, C.D. Ma, et al., A novel in-situ stress measurement method incorporating non-oriented core ground re-orientation and acoustic emission: A case study of a deep borehole, Int. J. Rock Mech. Min. Sci. 152 (2022) 105079.
[40] T. Backers, S. Kattenbeck, D. Mandy, The Brown-Hoek stress-depth relation revisited, in: 15th ISRM Congress, Salzburg, Austria (2023).
[41] Y. Zhang, X.T. Feng, C.X. Yang, et al., Evaluation method of rock brittleness under true triaxial stress states based on pre-peak deformation characteristic and post-peak energy evolution, Rock Mech. Rock Eng. 54 (2021) 1277–1291.
[42] M.D. Kuruppu, Y. Obara, M.R. Ayatollahi, et al., ISRM-suggested method for determining the mode I static fracture toughness using semi-circular bend specimen, Rock Mech. Rock Eng. 47 (2014) 267–274.
[43] M.R. Ayatollahi, E. Mahdavi, M.J. Alborz, et al., Stress intensity factors of semi-circular bend specimens with straight-through and chevron notches, Rock Mech. Rock Eng. 49 (2016) 1161–1172.

Liangjie Gu is a Master's supervisor at Chengdu University of Technology. He is a Distinguished Research Fellow at the State Key Laboratory of Geohazard Prevention and Geoenvironment Protection. His research focuses on the failure mechanisms and early warning strategies for deep hard rock engineering and excavated slopes. He has published nearly 20 SCI papers in the last five years, holds 6 patents, and has registered 2 software copyrights. He has led several projects funded by the National Natural Science Foundation of China and the Sichuan Provincial Natural Science Foundation. He has received the First Prize of the Green Mine Science and Technology Award and is a reviewer for several renowned academic journals.